Positron Emission Tomography with [18F]-DPA-714 Unveils a Smoldering Component in Most Multiple Sclerosis Lesions which Drives Disease Progression

Mariem Hamzaoui, Jeanne Garcia, Giacomo Boffa, Andrea Lazzarotto, Martina Absinta, Vito A.G. Ricigliano, Theodore Soulier, Matteo Tonietto, Philippe Gervais, Anne Bissery, et al.

HAL Id: hal-04446362

https://hal.sorbonne-universite.fr/hal-04446362v1

Submitted on 8 Feb 2024

Positron Emission Tomography with [¹⁸F]-DPA-714 Unveils a Smoldering Component in Most Multiple Sclerosis Lesions which Drives Disease Progression

Mariem Hamzaoui, PhD [1], Jeanne Garcia, MD [1], Giacomo Boffa, MD, PhD [1,2]

Andrea Lazzarotto, MD, PhD [1,3] Martina Absinta, MD, PhD [4,5]

Vito A.G. Ricigliano, MD, PhD [1,3] Theodore Soulier, MD, PhD [1] Matteo Tonietto, PhD [1,6]

Philippe Gervais, PhD [6] Anne Bissery, MD [7] Céline Louapre, MD, PhD [1,8]

Michel Bottlaender, PhD [6] Benedetta Bodini, MD, PhD [1,3] and Bruno Stankoff, MD, PhD [1,3]

Objective: To determine the prognostic value of persisting neuroinflammation in multiple sclerosis (MS) lesions, we developed a 18 kDa-translocator-protein-positron emission tomography (PET) -based classification of each lesion according to innate immune cell content and localization. We assessed the respective predictive value of lesion phenotype and diffuse inflammation on atrophy and disability progression over 2 years.

Methods: Thirty-six people with MS (disease duration 9 ± 6 years; 12 with relapsing–remitting, 13 with secondary-progressive, and 11 with primary-progressive) and 19 healthy controls (HCs) underwent a dynamic [¹⁸F]-DPA-714-PET. At baseline and after 2 years, the patients also underwent a magnetic resonance imaging (MRI) and neurological examination. Based on a threshold of significant inflammation defined by a comparison of [¹⁸F]-DPA-714 binding between patients with MS and HCs, white matter lesions were classified as homogeneously active (active center), rim-active (inactive center and active periphery), or nonactive. Longitudinal cortical atrophy was measured using Jacobian integration.

Results: Patients with MS had higher innate inflammation in normal-appearing white matter (NAWM) and cortex than HCs (respective standardized effect size = 1.15, 0.89, $p = 0.003$ and < 0.001). Out of 1,335 non-gadolinium-enhancing lesions, 53% were classified as homogeneously-active (median = 17 per patient with MS), 6% rim-active (median = 1 per patient with MS), and 41% non-active (median = 14 per patient with MS). The number of homogenously-active lesions was the strongest predictor of longitudinal changes, associating with cortical atrophy ($\beta = 0.49$, $p = 0.023$) and Expanded Disability Status Scale (EDSS) changes ($\beta = 0.35$, $p = 0.023$) over 2 years. NAWM and cortical binding were not associated to volumetric and clinical changes.

Interpretation: The [¹⁸F]-DPA-714-PET revealed that an unexpectedly high proportion of MS lesions have a smoldering component, which predicts atrophy and clinical progression. This suggests that following the acute phase, most lesions develop a chronic inflammatory component, promoting neurodegeneration and clinical progression.

ANN NEUROL 2023;94:366–383

Introduction

In multiple sclerosis (MS), neurodegeneration is known to start at the earliest stage of the disease course,[1] and to largely progress independently of acute inflammation driven by adaptive immune system activation.[1–4] Understanding and monitoring in vivo the mechanisms involved in neurodegeneration, as well as identifying effective predictors of individual trajectories of clinical evolution in patients with MS remain major challenges.

Innate immune cell-mediated neuroinflammation, involving mainly microglia, is considered to play a central role in the neurodegenerative process in MS.[5] Following the acute inflammatory demyelinating phase at lesion onset, each MS lesion may undergo several fates over time: (i) inflammation resolution and irreversible demyelination ("inactive lesions"); (ii) efficient myelin repair ("remyelinated lesions"), possibly facilitated by pro-regenerative microglia,[6] and (iii) long-term persistence of microglia-induced neuroinflammation leading to chronic active lesions (CALs).[5,7,8] In chronically inflamed lesions, that have been referred to as "mixed active/inactive"[5] or "slowly expanding/smoldering,"[7] the persistence of activated microglia can be extensive throughout the lesion[5] or remain confined at the lesion border, with the center of the plaque being hypocellular.[7] This part of chronic innate immune cells activation within a given lesion has been named "smoldering," referring to its suggested role in promoting ongoing active demyelination after the acute inflammatory stage of lesions.[9] The mechanisms involved in the persistence of neuroinflammation are still poorly known,[10,11] but choroid plexuses,[12] which have been shown to be enlarged and inflamed in patients with MS with inflammatory profiles,[13,14] may contribute to this process. Although radiological detection of CAL is extremely challenging on conventional magnetic resonance imaging (MRI), some of these lesions are accessible to emerging non-conventional MRI techniques,[15–17] including susceptibility-sensitive imaging.

Positron emission tomography (PET) with radiotracers targeting the 18-kDA translocator protein (TSPO) opens the perspective to selectively quantify innate immune cell density in the central nervous system.[18,19] Studies applying TSPO radiopharmaceuticals in MS have demonstrated an increased binding in lesions and normal-appearing tissues of patients with MS compared with healthy controls (HCs)[20–22] that correlate with disease severity.[20–25] A few studies have suggested that TSPO-PET could be used to identify CALs, which could be found at every stage of the disease.[22,25,26] However, the longitudinal prognostic value of different lesional stages identified by PET remains poorly explored.

Here, we developed a novel PET-based classification of MS lesions based on their innate immune cell content and localization using [18F]-DPA-714[25,27] a fluorinated second-generation TSPO radiopharmaceutical. Our objective was to prospectively investigate the predictive role of lesion phenotypes and diffuse neuroinflammation on brain atrophy and disability progression over 2 years.

Methods

Study Population

Forty-one patients with MS according to the 2005 revised McDonald criteria[28] (13 with relapsing–remitting multiple sclerosis [RRMS], 15 with secondary-progressive multiple sclerosis [SPMS], and 13 with primary-progressive multiple sclerosis [PPMS]) and 20 age- and sex-matched healthy controls (HCs) were enrolled in this 2-year longitudinal study. All subjects gave written informed consent to participate in a protocol approved by the local ethics committee (National Clinical Trial [NCT] NCT02305264).

The subjects were genotyped for the rs6971 polymorphism which affects TSPO binding.[29] Subjects were categorized as either having high-affinity binding (HAB), mixed-affinity binding (MAB), or low-affinity binding to TSPO sites. The latter group as well as one patient with motion artifacts were excluded from further analysis resulting in 36 patients (58% women; 12 with RRMS, 13 with SPMS, and 11 with PPMS) analyzed at baseline. Seven patients (5 with RRMS, 1 with SPMS, and 1 with PPMS) withdrew from the longitudinal MRI study, and one MRI scan at follow-up was excluded due to motion artifacts (1 SPMS; Figure 1).

Clinical Assessment

At study entry and after 2 years, patients underwent a neurologic examination and were assessed using the Expanded Disability Status Scale (EDSS)[30] and Symbol Digit Modalities Test (SDMT).[30] Prospective clinical changes over follow-up for SDMT (Δ-SDMT) were calculated subtracting the scores at study entry from the ones measured after the 2-year follow-up. In the case of the EDSS, we calculated the EDSS-stepwise-change, which is the difference between the score at the 2 visits, doubled if the baseline EDSS exceeded 5.5, due to nonlinearity of the scale.[31] Ongoing disease-modifying treatments were recorded and patients with MS were grouped into 3 classes according to treatment efficacy (untreated, low-efficacy, and high-efficacy; Table 1).
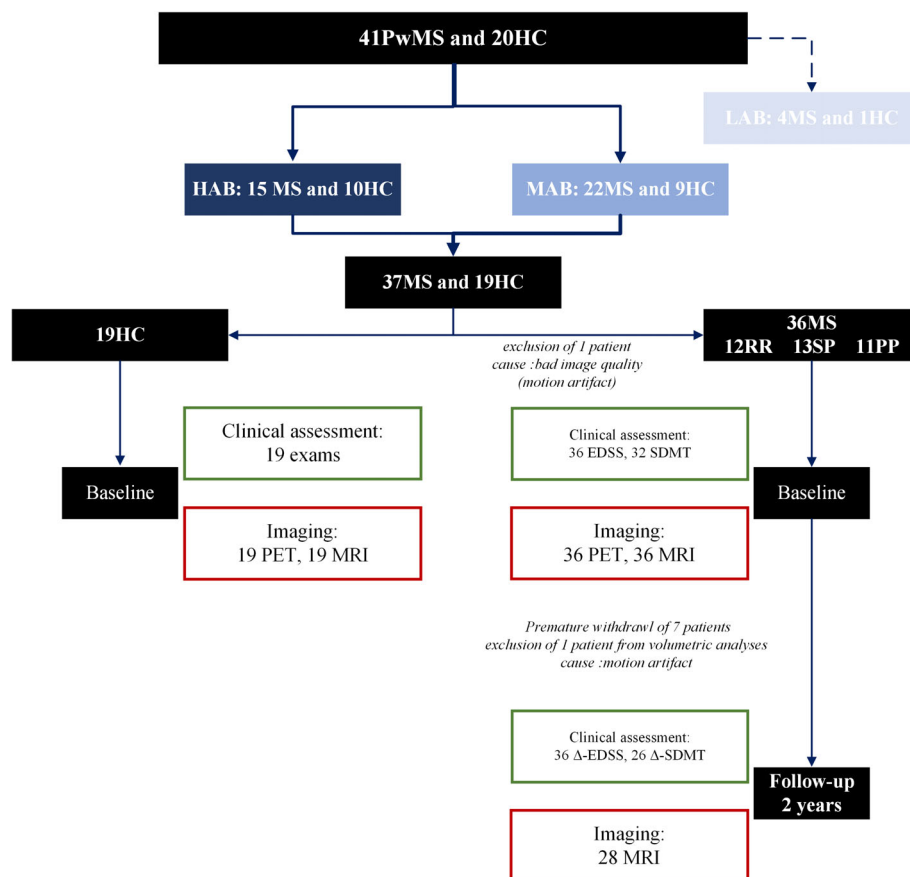
FIGURE 1: Study flow chart. EDSS = Expanded Disability Status Scale; HAB = high affinity binding; HC = healthy controls; LAB = low affinity binding; MAB = medium affinity binding; MRI = magnetic resonance imaging; MS = multiple sclerosis; MSFC = Multiple Sclerosis Functional Composite; PET = positron emission tomography; PP = primary progressive; RR = relapsing remitting; SDMT = symbol digit modalities test; SP = secondary progressive. [Color figure can be viewed at www.annalsofneurology.org]

Image Acquisition

All subjects underwent MRI (3-T Prisma with a 32-channel head coil; Siemens) and dynamic $[^{18}F]$-DPA-714 PET (High Resolution Research Tomograph; Siemens) at study entry. In addition, patients with MS underwent a follow-up MRI after 2 years. The MRI protocol included the following sequences: 3-dimensional T1-weighted magnetization-prepared rapid gradient-echo (3D-T1 MPRAGE, TR/TE 2300/2.98 ms, inversion time 900 ms, resolution $1.0 \times 1.0 \times 1.1$ mm^3), T2-weighted (T2-w, TR/TE 4000/83 ms, resolution $0.9 \times 0.9 \times 3.0$ mm^3), 3-dimensional fluid-attenuated inversion recovery (FLAIR, TR/TE 8880/129 ms, resolution $0.9 \times 0.9 \times 3.0$ mm^3), and pre- and post-gadolinium (gadoteric acid, 0.2 ml/kg) T1-weighted spin-echo (T1SE, TR/TE 650/14 ms resolution, $1.0 \times 1.0 \times 3.0$ mm^3).

The PET protocol consisted of an intravenous bolus injection of 198.4 ± 22.9 MBq of $[^{18}F]$-DPA-714 at the beginning of a 90-minute dynamic acquisition[27]. Images were reconstructed using the 3D ordinary Poisson ordered subset expectation maximization algorithm and the point spread function was modeled within the reconstruction to minimize partial volume effect (PVE).

Image Post-Processing
MR Image Processing

i. Lesion contouring and individualization: In patients with MS, hyperintense white matter (WM) lesions were manually segmented on T2-w scans with reference to FLAIR images using Jim (version 6.0, http://www.xinapse.com/). To improve individual lesion detection within an area of confluence, we implemented a recently described method.[32] For each patient, we generated a probability mask based on the T2-w intensity of each lesional voxel, which reflects its probability to be in a lesion. To exclude voxels with low probability to be lesional, we applied a threshold (0.25) identified and validated by 2 neurologists (authors J.G. and B.B.) after visual inspection. Isolated nonconfluent lesions, defined as lesions smaller than 300 mm^3 (threshold selected based on the distribution of lesions volume in

TABLE 1. Demographic, clinical, and imaging characteristics of patients and healthy controls

Characteristics	HCs	Patients (all)	RRMS	SPMS	PPMS
Distribution	19	36	12	13	11
Age	47 ± 14	48 ± 11 (N.S.)	44 ± 14	52 ± 9	48 ± 10
Disease duration	-	9 ± 6	6 ± 4	14 ± 6	7 ± 3
F/M	13/6	21/15 (N.S.)	9/3	9/4	3/8
Genotype (MAB/HAB)	9/10	15/21 (N.S.)	4/8	5/8	6/5
Disease modifying treatment (untreated/low- efficacy/high-efficacy)	-	18/10/8	1/6/5	7/4/2	10/0/1
Clinical data		(mean ± SD)			
EDSS	-	4.5 ± 1.5	3.5 ± 1	5.5 ± 1	5.5 ± 1.5
SDMT (zs)	-	−1.74 ± 0.7	−1.59 ± 0.59	−2.17 ± 0.81	−1.48 ± 0.53
ROI Volume		Normalized by the eTiV (mean % ± SD %)			
Whole brain without ventricles volume	64 ± 2	62 ± 3 (***)	63 ± 4	60 ± 2	63 ± 3
WM volume	31 ± 1.86	29.39 ± 2.34 (**)	29.11 ± 2.55	28.35 ± 1.59	30.93 ± 2.22
TGM volume	35.28 ± 1.8	33.49 ± 1.93 (**)	34.53 ± 2.25	32.97 ± 1.53	32.97 ± 1.66
Cortical volume	31.73 ± 1.72	30.33 ± 1.83 (**)	31.39 ± 2.04	29.96 ± 1.46	29.61 ± 1.58
Inflammation markers		DVR (mean ± SD)			
DVR TWM	0.92 ± 0.07	0.97 ± 0.08 (**)	0.95 ± 0.07	0.99 ± 0.08	0.98 ± 0.07
DVR NAWM	-	0.97 ± 0.08	0.95 ± 0.07	0.99 ± 0.08	0.98 ± 0.08
DVR lesions	-	0.94 ± 0.12	0.92 ± 0.11	0.94 ± 0.16	0.95 ± 0.09
DVR TGM	1.55 ± 0.09	1.63 ± 0.13 (*)	1.63 ± 0.17	1.62 ± 0.12	1.63 ± 0.08
DVR cortex	1.53 ± 0.08	1.65 ± 0.14 (***)	1.65 ± 0.18	1.65 ± 0.13	1.66 ± 0.08
Lesions analyses		(mean ± SD)			
Lesion load (cm^3)	-	18.4 ± 12.83	15.9 ± 10.69	21.6 ± 12.56	17.33 ± 15.47
No. lesions	-	37 ± 27	31 ± 21	45 ± 29	35 ± 29
No. homogeneously active lesions	-	19.81 ± 19.15	15.08 ± 17.86	27.15 ± 23.86	16.27 ± 11.8
No. rim active lesions	-	2.19 ± 2.85	1.42 ± 2.39	3 ± 3.27	2.09 ± 2.77
No. nonactive lesions	-	15.08 ± 12.59	14.08 ± 7.38	14.77 ± 11.17	16.55 ± 18.48

Note: Linear models were corrected for the TSPO genotype, and significance is shown for differences between HCs and the whole group of patients. Low-efficacy treatments refer to glatiramer acetate, teriflunomide, interferon, and dimethyl fumarate; high-efficacy treatments refer to fingolimod, natalizumab, ocrelizumab, rituximab, alemtuzumab, and mitoxantrone.

N.S. $p > 0.05$.

*$p < 0.05$,

**$p < 0.01$.

***$p < 0.001$.

Abbreviation: DVR = distribution volume ratio; EDSS = Expanded Disability Status Scale; eTiV = estimated total intracranial volume; HCs = healthy controls; NAWM = normal appearing white matter; N.S. = not significant; PPMS = primary-progressive; ROI = region of interest; RRMS = relapsing-remitting multiple sclerosis; SDMT = Symbol Digit Modalities Test; SPMS = secondary-progressive multiple sclerosis; TGM = total grey matter; TWM = total white matter; WM = white matter.

our cohort), were identified after labeling the entire mask. To separate a confluent lesion into individual lesions, we calculated the hessian matrix for each voxel in the thresholded probability mask with the aim to identify clusters resembling the center of each lesion.[32] Lesional centers were then labeled and propagated through the refined binary mask. After manual correction, a final labeled lesion mask was obtained (Figure 2A). This procedure resulted in the splitting of 105 confluent lesions (median volume = 2515 mm^3, range = 407–43,813 mm^3).

ii. Regions of interest and registration to standard space: Binarized lesion masks were aligned to the 3D-T1 MPRAGE scans using Advanced Normalization Tools (ANTs; http://stnava.github.io/ANTs/). After "lesion filling," the segmentation of total grey matter (TGM), cerebral cortex, total white matter (TWM), and cerebral spinal fluid (CSF) was performed on 3D-T1 MPRAGE scans using Freesurfer6 (http://surfer.nmr.mgh.harvard.edu/), and the total intercranial volume (TIV) was estimated. In all subjects, choroid plexuses (CPs) were segmented manually on the 3D-T1 MPRAGE.[13] In each subject, we then defined the following regions of interest (ROIs) on 3D-T1 MPRAGE scans: (i) TWM, (ii) cortex, (iii) CP, and (iv) the whole brain without ventricles. For patients with MS, 2 additional ROIs were defined: (i) T2-w lesions and (ii) normal-appearing WM (NAWM), defined as the TWM eroded by 2 mm from the grey matter (GM), ventricles, and T2-w lesions. In each subject, we used ANTs to perform a 3-level registration (rigid, affine, and diffeomorphic) of the 3D-T1 MPRAGE onto a standard brain image (Montreal Neurological Institute [MNI152 09c sym]), which was then used to align all ROIs to standard space.

PET Quantification and Image Processing. Voxel-wise [18F]-DPA-714 distribution volume ratio (DVR) parametric maps were obtained using the Logan graphical analysis based on a reference region, which was extracted using a supervised clustering algorithm[27] in the cerebral cortex.[25] DVR maps were co-registered to the 3D-T1 MPRAGE images and then normalized to MNI.

Mean DVR values were then extracted from each ROI, after partial volume correction of the DVR signal using the Muller-Gartner method (PETPVC) for the cerebral cortex.

Lesion Classification Based on [18F]-DPA-714 Binding. The [18F]-DPA-714 binding was separately calculated in the center and in the rim of each lesion in standard space. The center of each lesion was defined as the lesion eroded by a spheric kernel of 1 mm. The rim of each lesion was obtained by dilating the lesion using a spheric kernel of 2 mm and then subtracting the previously defined center, thus generating a 3 mm width rim. To ensure that lesional rims did not overlap with neighboring lesions, only rims belonging to free lesion edges were retained within the rim mask (Figure 2B). To minimize PVE, voxels localized less than 2 mm far from ventricles and from cortex were removed from further analysis and only lesions having both center and rim volume above 50 voxels were retained. Gadolinium enhancing lesions were excluded to avoid bias due to blood brain barrier breakdown.

To define pathological DVR values, we have followed a 2-step procedure to allow the selection of a conservative threshold.

First, we characterize the intersubject variability of the PET signal among HCs by running a "one versus all" analysis of [18F]-DPA-714 DVR, taking into account their *TSPO* genotype. This analysis was conducted specifically in a WM ROI that reproduced the mean lesion mask of the patients included in the study. We obtained a mean distance between single subject and group values of [18F]-DPA-714 DVR of 0.19% with a standard deviation of 13.98%. This indicated that, according to intersubject variability among controls, the threshold should be above 14.2%.

Second, we characterized regions of significant differences in [18F]-DPA-714 DVR maps between controls and patients by applying a permutation-based *t* test with threshold-free cluster free enhancement using Randomize from FSL library, including age, sex, and *TSPO* genotype as covariates. This step generated an ROI in which patients' [18F]-DPA-714 DVR was significantly higher compared to controls. Then, we defined the threshold by calculating the percent difference between the mean [18F]-DPA-714 DVR in the ROI of significant difference between patients and HCs. This yielded a threshold of significance at 18.31%.

Taking into consideration the 2 steps, and with the objective of being conservative, we then rounded the threshold at 20%.

Therefore, comparing a patient with HCs with the same genotype, we classified an area (rim/center) as "active" if its mean DVR signal was higher than 20% of the mean WM DVR signal of HCs covered by that area.

We thus obtained 3 subtypes of lesions (Figure 2C):

- **Homogeneously-active lesion** when the center of the lesion was classified as "active" regardless of the classification of the corresponding rim.
- **Rim-active lesion** when the rim was classified as "active", but no activation was identified in the corresponding lesion center.
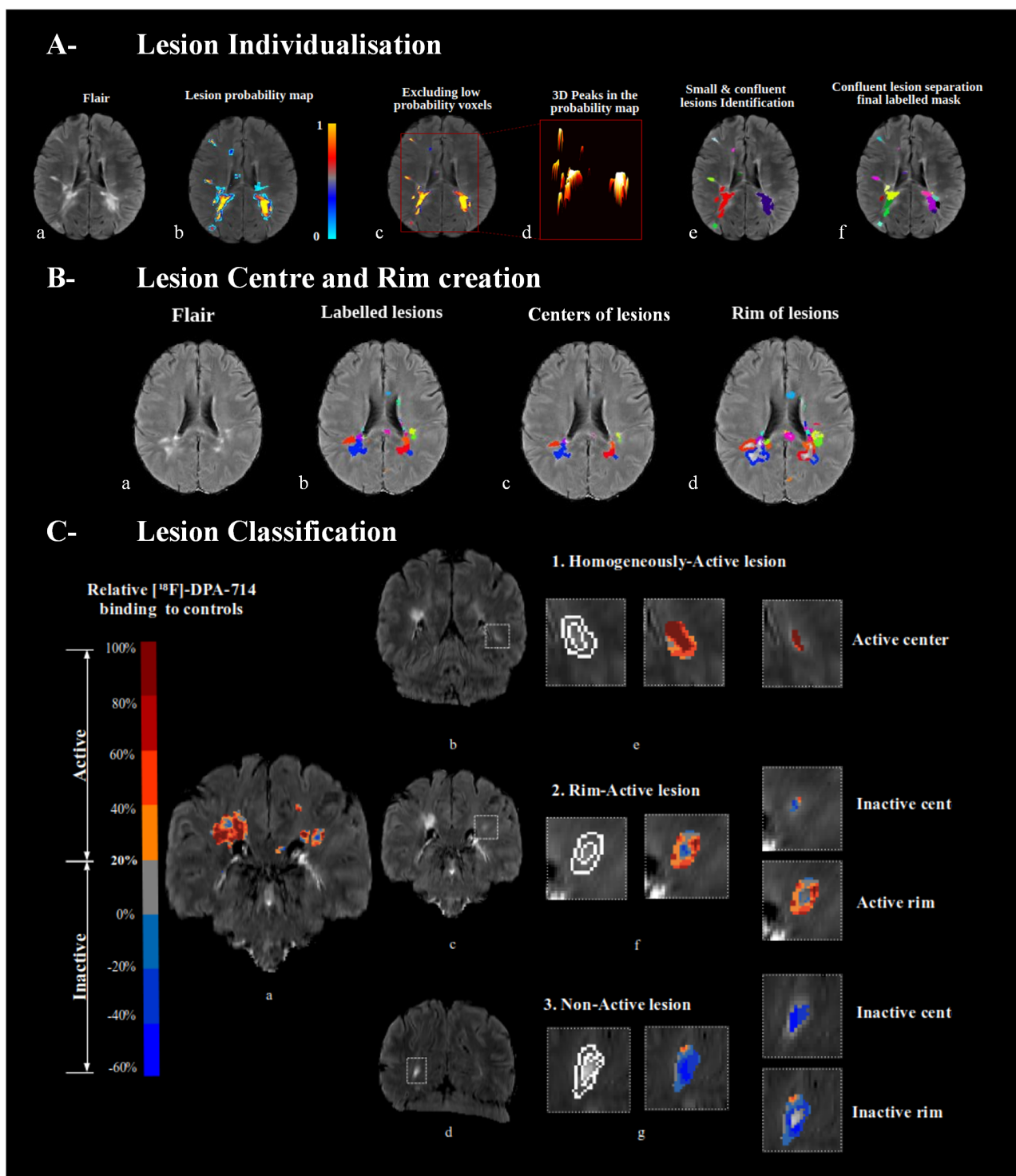
FIGURE 2: White matter lesion classification according to MRI and [18F]-DPA-714. **(A)** Lesion individualization. **(a)** An illustrative FLAIR axial slice from a subject with MS who showed confluent lesions. **(b)** Lesion probability map based on T2-w intensity: the intensity represents a voxel's probability to be included in a lesion, where higher values are in hot colors. **(c)** Elimination of voxels with a low probability under 0.25 (blue voxels). **(d)** The 3D representation of lesions, the centers of lesions appearing as peaks. **(e)** Small and confluent lesion identification (volume threshold of confluence definition 300 mm³) and small lesion labeling. **(f)** Final labeled lesion mask, after confluent lesion separation using centers identification and label attribution with respect to small lesions, each color representing a lesion. **(B)** Lesion center and rim creation. **(a)** An illustrative FLAIR axial slice from a subject with MS. **(b)** Labeled lesion mask. **(c)** Lesion centers mask obtained by eroding the lesion mask for a spherical kernel of 1 mm. **(d)** Lesion rims mask obtained after dilating the lesion mask by a spherical kernel of 2 mm, subtracting the lesion centers mask to the dilated one. In the final mask, only the rim areas with no overlap with neighboring lesions were kept. **(C)** Lesion *(Figure legend continues on next page.)*

- **Non-active lesion** when neither its center nor its rim was classified as "active."

The 3D masks of each lesion subtype of all the patients were averaged to obtain a lesion probability map for each lesion class.

Volumetric Assessment. To allow volume comparisons between subjects, volumes of ROIs were normalized to TIV.

Volumetric changes after 2 years were assessed using the Jacobian integration method.[33] This method is based on the coregistration of 3D-T1 MPRAGE images on their halfway-space and on the calculation of a Jacobian determinant map from the nonlinear deformation field between timepoints. Atrophy was obtained averaging the voxels of the Jacobian map within each ROI (higher values reflecting greater volume loss).

TSPO Gene Expression in Single-Nucleus Transcriptomics of MS Brain Tissue. The FASTQ files and metadata of 3 published single-nucleus RNAseq studies[34–36] were downloaded from GEO or SRA repositories (accession number GSE118257, PRJNA544731, and GSE180759, respectively). They included a total of 123,193 nuclei from 21 progressive MS cases (10 women, mean age = 46.7 years, age range = 34–58 years) and 17 non-neurological controls (6 women, mean age = 55 years, age range = 34–82 years). Snap-frozen brain samples from MS autopsy cases were classified based on the presence of lesions at different pathological stages. Single-nucleus RNAseq datasets were analyzed individually using the same bioinformatic pipeline (Seurat version 4 R-based package), as previously described in detail.[36] For each dataset, Uniform Manifold Approximation and Projection (UMAP) plots were generated, and cell-type annotation were performed using known lineage markers and compared to the results from original publications. To assess *TSPO* cellular specificity, average *TSPO* expression and z-scores were computed from each cell cluster for each dataset. We then performed a subclustering analysis of immune cells and astrocytes in the dataset with the highest number of glial nuclei[36] to identify which glial phenotypes showed highest *TSPO* expression; average

TSPO expression and z-scores were computed from each cell subcluster.

Statistical Analyses

Statistical analyses were performed in STATA (version 14.0), considering 2-sided $p < 0.05$ as significance level. Corrections for multiple comparisons were performed using the false discovery rate.

Differences in mean DVR between the ROIs in HCs and in patients with MS, and between ROIs of patients according to MS subgroups and sex, were assessed using linear models corrected by the genotype followed by pairwise comparisons.

Associations among each of the 3 lesion subtypes and clinical and demographic variables were tested using multivariable linear regression models, with the number of each lesion subtype included as the response variable, and sex, age, disease duration, MS subgroups, and treatment as explanatory variables.

The spatial distribution of lesion subtype was examined by visual inspection of lesion probability maps. In addition, to explore the association between the distribution of lesion subtypes in the WM and in the first periventricular rim (3–6 mm from ventricles[37]) and the choroid plexus volume, we used linear models adjusted by ventricular volume.

The association between immune inflammation markers and volumetric/clinical variables was investigated at study entry and after 2 years of follow-up using multiple ordered logistic regression models or multivariable linear regression models depending on the continuity of the response variables except in the case of nonapplicability of the model (non-normal residual distribution). In that case, correlations (Spearman or Pearson depending on the normality of the variables) were given when significant. In the main analysis, all regressions were adjusted for sex, disease duration, and treatment type. An additional correction for the genotype was applied when raw DVR values were predictors of interests.

The included predictors of interests were number of homogeneously active lesions, number of rim-active lesions, number of nonactive lesions, mean DVR of NAWM, and mean DVR of cortex.

---

classification. (a) The [18F]-DPA-714 binding changes between white matter lesions and corresponding areas in the white matter of controls, superimposed on the coronal FLAIR MRI slice, from a subject with MS: a threshold of 20% (hot colors) defines areas of pathological inflammation in patients. (b, c, d) Three illustrative MRI coronal FLAIR slices pointing lesions of interest in the white matter. (e, f, g) Delineation of the center and rim of each lesion on FLAIR slices, and their corresponding [18F]-DPA-714 binding changes, allowing to identify "homogeneously active" lesions with centers classified as "active," "rim active" lesions with center classified as "inactive" and rim as "active," and "nonactive" lesions with both centers and rim classified as "inactive." FLAIR = fluid-attenuated inversion recovery; MRI = magnetic resonance imaging; MS = multiple sclerosis. [Color figure can be viewed at www.annalsofneurology.org]

The volumetric response variables included were the normalized volume of the whole brain without ventricles and the cortex volume at study entry, and their respective volume changes after 2 years. The clinical response variables were the raw EDSS and 2 years EDSS stepwise change.

Based on the clinical and radiological markers, we also defined patients as presenting or not the following characteristics: (i) disability worsening if their EDSS stepwise change over the follow-up was > 0; (ii) moderate cognitive impairment if their z-score transformed SDMT at study entry was < -1.5SD[38]; (iii) cognitive worsening if their ΔSDMT < -4[39]; (iv) clinical relapse(s) over the follow-up; (v) radiological signs of ongoing inflammatory process defined as the appearance of new T2-w lesions or gadolinium enhancement during follow-up (identified by 2 neurologists [authors J.G. and B.B.] after visual inspection of the T2-w and T1SE pre and post-gadolinium); (vi) pathological cortical atrophy if their annual cortical volume loss rate was > 0.41% per year[40]; and (vii) pathological whole brain atrophy if their annual total brain volume loss rate was > 0.4% per year.[41]

Wilcoxon/t tests were performed for assessing differences in the studied variables among these groups.

The predictive value of PET-derived inflammation markers on longitudinal volumetric/clinical variables evolution was finally assessed in exploratory analysis: (i) in the subgroup of patients free of relapses during the follow-up; and (ii) taking into account baseline T2 lesion load and normalized brain volume. As lesion load is expressed as a volume, the included predictors of interest here were the volumes of homogeneously active lesions, rim-active lesions, and nonactive lesions. The response variables were the cortical volume change and EDSS-stepwise-change after 2 years; a first model was adjusted for T2 lesion volume and normalized brain volume at baseline only; a second model was adjusted for sex, disease duration, treatment type T2 lesion volume, and normalized brain volume at baseline.

Results

Demographic and clinical characteristics are reported in Table 1.

People with MS Have a Higher Brain Neuroinflammation Compared to Healthy Controls

At the whole-group level, patients with MS had a significantly higher mean DVR value in TGM, cortex, and NAWM than HCs (respectively, standardized effect size = 0.716, 1.15, 0.892; $p = 0.015$, < 0.001, and 0.003; see Table 1), the difference being more pronounced in patients in the progressive phases compared to HCs (respectively, standardized effect size = 0.796, 1.25, and 1.078; $p = 0.035$, < 0.001, and 0.0026). For patients with MS, there were no differences in these regions according to disease phenotype or sex.

The mean DVR in lesions of patients with MS was not significantly different from the mean DVR of TWM of HCs. The global lesional DVR was significantly lower in women compared with men (mean female [HAB and MAB] = 0.89, 0.92, mean male [HAB and MAB] = 0.93, 1.06, and standardized effect size = 0.713, $p = 0.0432$), but did not differ across disease phenotypes.

[¹⁸F]-DPA-714 PET Reveals an Extended Smoldering Component in MS Lesions

Following the exclusion of small lesions (center or rim < 50 mm³) and gadolinium-positive lesions (34 lesions), we could analyze 1,335 individual lesions. Out of these, 53% were classified as homogeneously-active (mean volume = 537.7 mm³ ± 497.4), 6% as rim-active (mean volume = 425.5 mm³ ± 314.9), and 41% as non-active (mean volume = 488 mm³ ± 446.6). We identified a mean of 20 homogeneously active, 2 rim-active and 15 non-active per patient (see Table 1). Fifteen patients did not have any rim-active lesion (6 with RRMS, 4 with SPMS, and 5 with PPMS), and only 3 did not have any homogeneously-active lesion (1 with RRMS and 2 with SPMS).

Non-active lesions were significantly more frequent in women than men (mean female = 18.7, mean male = 10, $p = 0.036$), whereas no sex difference was detected for homogeneously-active ($p = 0.295$) and rim-active ($p = 0.513$) lesions.

Patients with progressive MS had more homogeneously-active ($p = 0.032$) and rim-active lesions ($p = 0.006$) than patients with RRMS, whereas the total lesion load was not significantly different between these groups ($p = 0.081$). The number of rim-active lesions was higher in patients with SPMS than in patients with RRMS (mean number in RRMS, SPMS, and PPMS, respectively, 1.4, 3, and 2.1; $p = 0.026$ between RRMS and SPMS; Figure 3B). Lesion subtype repartition did not differ between patients with (n = 9) or without radiological activity, or between patients presenting relapse(s) (n = 6) or not during follow-up. When the number of each lesion subtype was normalized to the total number of T2 lesions the difference between the PMS and RRMS groups was not significant (percentage of homogeneously active lesions = 41.5 ± 24.6 in the RRMS group, 49.2 ± 26.1 in the PMS group, $p = 0.4$; percentage of rim active lesions = 4.1 ± 5.8 in the RRMS group, and 6 ± 7.6 in the PMS group, $p = 0.22$). Of note the numbers of T2 lesions
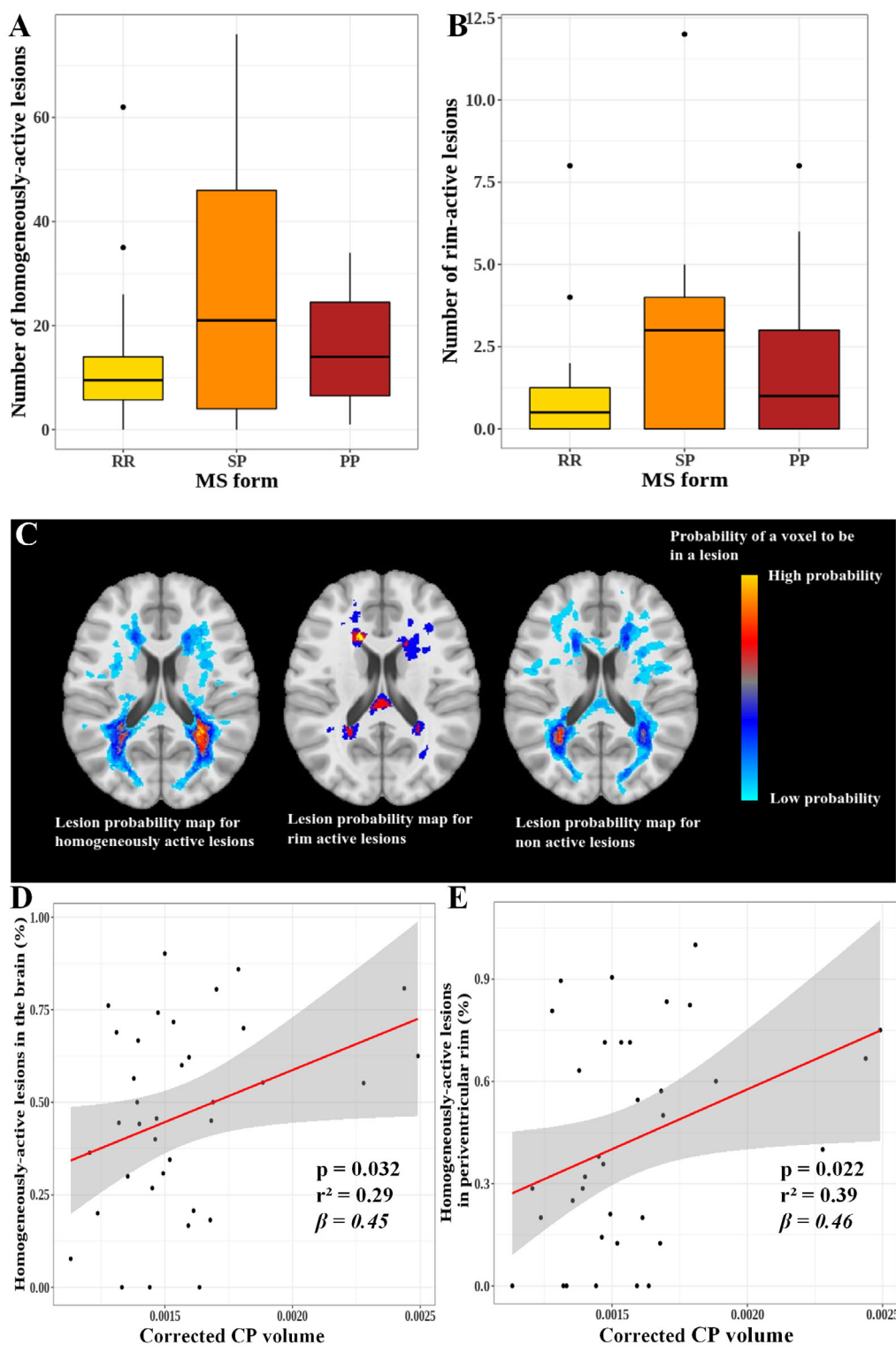
FIGURE 3: Individual and anatomic repartition of white matter lesions with a smoldering component. Box plot describing the repartition among MS forms of homogeneously active lesions (A) and rim active lesions (B). (C) Probability maps describing spatial disposition of lesions subtypes, from left to right: homogeneously active, rim active, and nonactive lesions. Hot colors represent a higher probability to be included in a lesion according to its subtype. Regression graphs showing the correlation between the corrected choroid plexus (CP) volume and the percentage of homogeneously active lesions in the entire white matter (D) and in the first periventricular rim, defined as 3–6 mm from the ventricles (E). MS = multiple sclerosis; RR =relapsing remitting; PP =primary progressive; SP =secondary progressive. [Color figure can be viewed at www.annalsofneurology.org]

showed great variations across subjects (mean $= 37 \pm 27$ per patient, range $= 3$–106).

A trend toward an association between older age and an increased number of rim-active lesions was observed ($p = 0.058$). We did not find any association between lesion subtype number and disease duration or treatment type.

After visual inspection of the 3 lesion probability maps (see Figure 3C), we found that, compared to non-active lesions, homogeneously-active and rim-active lesions were preferentially distributed in periventricular regions. A larger CP volume was significantly associated with a higher percentage of homogeneously active lesions in the whole WM ($β = 0.45$, $p = 0.032$; see Figure 3D), this association being stronger in the first periventricular WM rim ($β = 0.46$, $p = 0.022$; see Figure 3E).

The Lesional Smoldering Component Is Associated with Brain Atrophy

At baseline, higher DVR values in the cortex and NAWM were correlated with reduced cortical volume (Table 2: cortex: $β = -0.6$, $p = 0.015$ and NAWM: $β = -0.47$, $p = 0.027$). A higher rim-active lesion number correlated with a reduced baseline cortical volume (Table 3: rho $= -0.35$, $p = 0.039$), but not with total brain volume (Table 2: $p = 0.21$). Brain and cortical volumes were neither associated with the number of homogeneously-active nor with non-active lesions.

In the longitudinal analysis, there was no correlation between the mean DVR of NAWM and cortex with atrophy progression over the follow-up. A higher number of homogeneously-active lesions was associated with a more severe brain atrophy ($β = 0.44$, $p = 0.023$) and cortical atrophy ($β = 0.49$, $p = 0.023$) developing over 2 years (Figure 4C). The association between the number of homogeneously-active lesions and brain atrophy remained significant in the subgroup of relapse-free patients ($n = 30$, $β = 0.54$, $p = 0.008$). Patients with pathological cortical atrophy (defined as atrophy rate > 0.41% per year[40]) had a higher number of homogeneously active lesions at baseline compared to patients without pathological cortical atrophy (medians, respectively: 27.5 and 10, $p = 0.025$; see Figure 4E), but no difference in lesion subtype was found between patients with pathological whole brain atrophy (defined as annual total brain volume loss rate > 0.4% per year[41]) or without. Although the number of rim-active lesions was not associated with total brain atrophy developing over the follow-up (see Figure 4D), we found that this type of lesions was more frequent in patients who developed pathological cortical atrophy after 2 years compared with the rest of the patient cohort (medians, respectively: 4 and 0.5, $p = 0.038$; see

Figure 4F). Non-active lesions were not associated with any longitudinal volume change.

The results of the main regression models are detailed in Table 2 and, in case of nonapplicability of the regression, correlations are detailed in Table 3.

In the exploratory analysis adjusted for T2 lesion load and brain normalized volume at baseline, both the volume of homogeneously-active and of rim-active lesions at baseline correlated with cortical volume change at 2 years ($β = 1.45$, $p = 8 \times 10^{-5}$ and $β = 0.78$, $p = 0.041$, respectively). When the model was also adjusted for sex, disease duration, and treatment, only homogeneously-active lesion volume significantly correlated with cortical volume change at 2 years ($β = 1.71$, $p = 0.0001$).

The Lesional Smoldering Component Is Associated with Disability Progression

At baseline, mean DVR values of NAWM and cortex did not correlate with disability measures. When we looked at lesion subtypes, we found that patients with cognitive impairment ($n = 13$) had a significantly higher number of homogeneously active lesions compared to cognitively preserved patients (mean cognitive impaired $= 25.16$, mean cognitive preserved $= 8.38$, $p = 0.028$). The number of homogeneously active lesions was not associated with EDSS ($p = 0.619$). In the whole cohort, the number of rim-active and nonactive lesions was not associated with any disability metric.

The longitudinal analysis showed that mean DVR values in NAWM and cortex were not correlated with any longitudinal disability measure. When we looked at lesion subtypes, we found that a higher number of homogeneously-active lesions was correlated with higher EDSS stepwise-change, both in the whole cohort ($β = 0.35$, $p = 0.023$) and in the relapse-free patient subgroup ($β = 0.43$, $p = 0.017$). Patients who experienced clinical worsening compared to clinically stable patients ($n = 16$) had a higher number of homogeneously-active lesions at baseline (medians, respectively: 28.5 and 9.5, $p = 0.013$; see Figure 4A). Neither rim-active nor non-active lesions correlated with changes of the EDSS over the follow-up.

We found no difference in any inflammation markers between patients with or without cognitive worsening.

In the exploratory analysis adjusted for T2 lesion load and brain normalized volume at baseline, the volume of homogeneously-active lesions at baseline correlated with 2 years EDSS step change ($β = 0.67$, $p = 0.015$). When the model was also adjusted for sex, disease duration, and treatment, the correlation did not reach significance ($β = 0.54$, $p = 0.065$).

TABLE 2. Association between inflammatory markers derived from PET, and MRI volumetry or clinical disability at baseline and after follow-up

	Homogeneously active (number)	Rim-active (number)	Nonactive (number)	DVR NAWM	DVR cortex
At baseline					
Brain volume	$p = 0.22$	$p = 0.21$	$p = 0.54$	$p = 0.104$	$p = 0.817$
Cortex volume	$p = 0.6105$	N.A.	$p = 0.56$	$p = 0.027$ $r^2 = 0.34$ $\beta = -0.47$	$p = 0.015$ $r^2 = 0.37$ $\beta = -0.6$
EDSS	$p = 0.619$	$p = 0.27$	$p = 0.54$	$p = 0.77$	$p = 0.534$
After 2 yr follow-up					
Brain atrophy	$p = 0.023$ $r^2 = 0.38$ $\beta = 0.44$	$p = 0.249$	$p = 0.843$	$p = 0.917$	$p = 0.27$
Cortical atrophy	$p = 0.023$ $r^2 = 0.28$ $\beta = 0.49$	$p = 0.353$	$p = 0.843$	$p = 0.917$	$p = 0.345$
EDSS-stepwise-change	$p = 0.023$ $r^2 = 0.13$ $\beta = 0.35$	$p = 0.526$	$p = 0.843$	$p = 0.917$	$p = 0.345$

Note: Associations were tested at baseline and after follow-up by multiple linear or logistic regression after adjustment on gender, disease duration and treatment type.

N.A. = the model is not applicable because of the non-normal distribution of its residuals, and the association has been tested using Spearman or Pearson test (see Table 3).

The *p* values are reported after FDR correction for multiple.

Abbreviation: DVR = distribution volume ratio; EDSS = Expanded Disability Status Scale; FDR = false discovery rate; MRI = magnetic resonance imaging; NAWM = normal appearing white matter; PET = positron emission tomography.

TABLE 3. Correlations between inflammatory markers derived from PET and cortical volume at baseline

	Homogeneously-active (no.)	Rim-active (no.)	Non-active (no.)	DVR NAWM	DVR cortex
Baseline					
Cortex volume	$p = 0.568$	$p = 0.039$ rho $= -0.35$	$p = 0.3789$	$p = 0.058$ r $= -0.319$	$p = 0.04$ r $= -0.333$

Note: r = when Pearson correlation is applied (both variables are normally distributed); rho = when spearman correlation is applied (non-normal distribution for one of the variables).

Abbreviation: DVR = distribution volume ratio; NAWM = normal appearing white matter; PET = positron emission tomography.

Cellular Origin of TSPO Gene Expression in the MS Brain

To improve our understanding of the cellular origin of TSPO expression in the MS brain, we re-analyzed 3 published single-nucleus RNAseq studies.[34–36] *TSPO* gene expression is shown on MS and control brain UMAP plots for each analyzed single-nucleus RNAseq dataset in Figure 5A–D. As expected, *TSPO* was mainly expressed by microglial cells, but could also be detected in endothelial cells, in a subset of astrocytes and in a small proportion of oligodendrocytes (see Figure 5A).
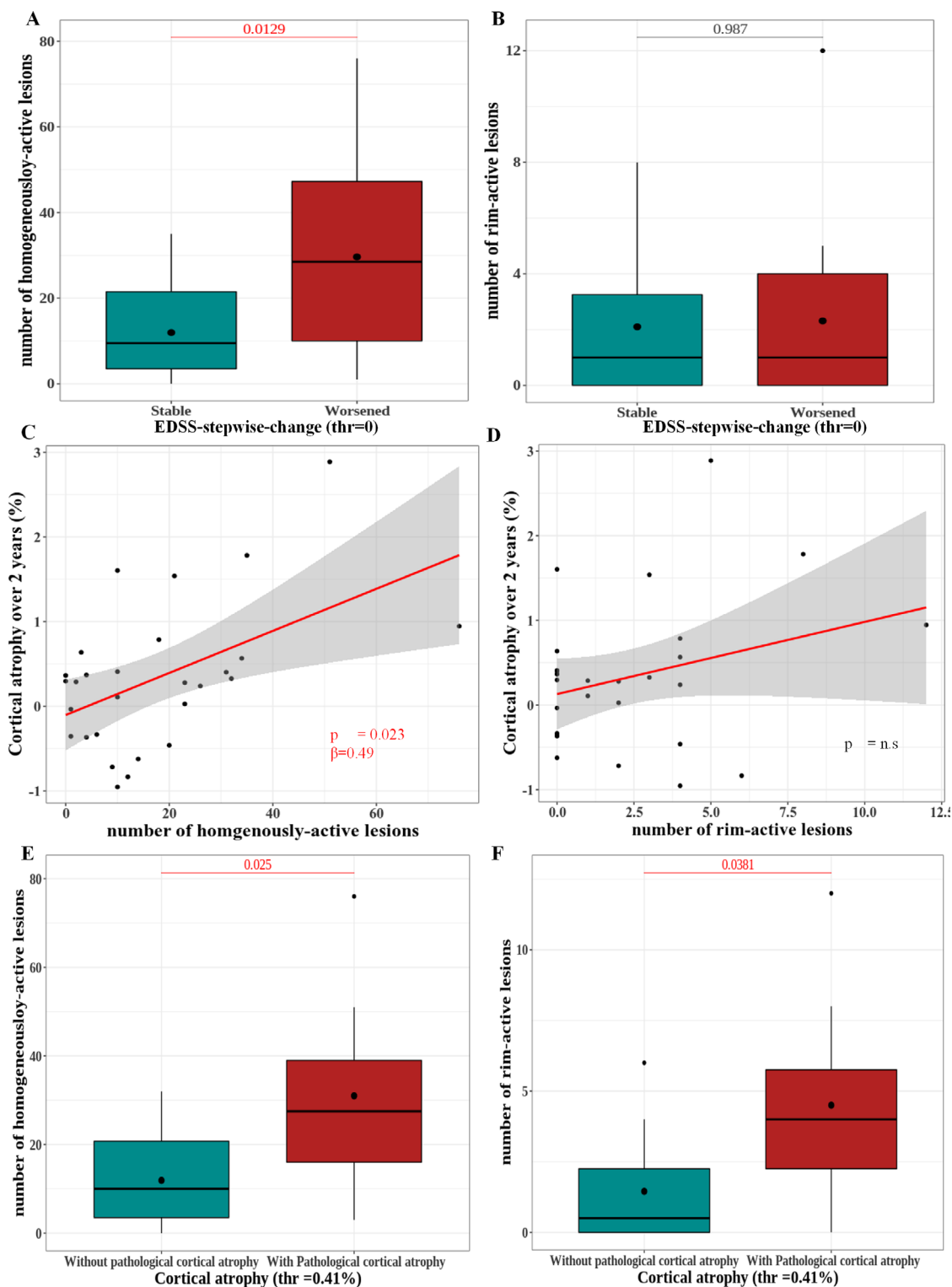
FIGURE 4: Homogeneously active lesions predict disease progression. Box plots showing the distribution of homogeneously active (A) and rim active (B) lesions according to EDSS stepwise change status: Stable or worsened. Regression graphs studying the association of cortical atrophy over 2 years with the number of homogeneously active lesions (C) and the number of rim active lesions (D). Box plots describing the distribution of homogeneously active (E) and rim active (F) lesions according to the presence of pathological cortical atrophy in patients. EDSS = Expanded Disability Status Scale. [Color figure can be viewed at www.annalsofneurology.org]

The subclustering analysis highlighted higher *TSPO* expression in activated microglia phenotypes, namely in microglia inflamed in MS (MIMS)-iron followed by MIMS-foamy (z-scores of 2.5 and 0.9, respectively, relative to all immune cells), as well as in neurodegenerative inflamed astrocytes (astrocytes
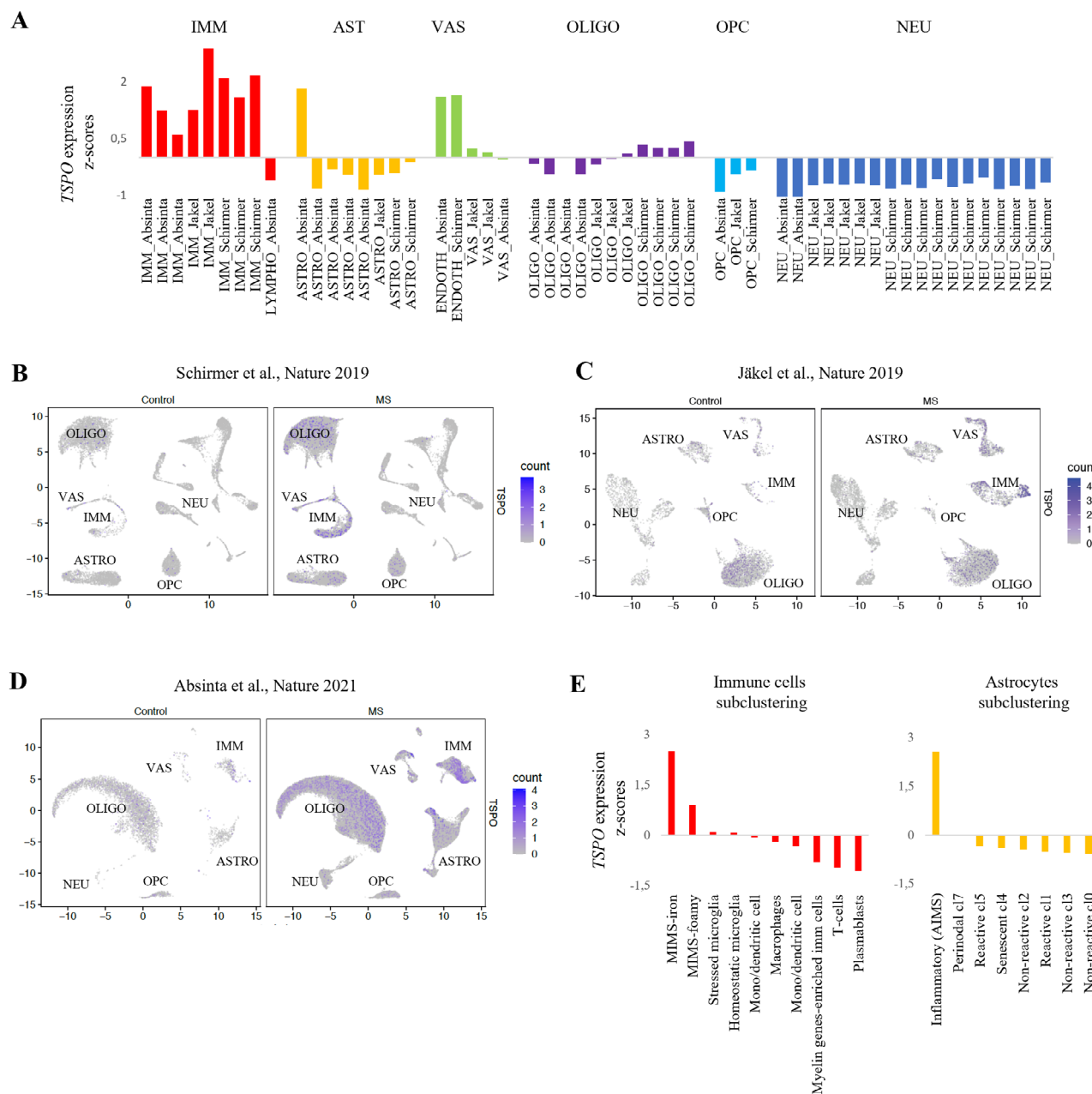
FIGURE 5: *TSPO* expression in single-nucleus transcriptomics of MS brain tissue. (A) *TSPO* gene expression z-scores by cluster. The source single-nucleus RNAseq dataset is retained in the cluster label. (B–D) Mapping *TSPO* gene counts (color-coded) on UMAP plots for MS versus control brain and for each single-nucleus RNAseq dataset. (E) *TSPO* gene expression z-scores by immune cells and by astrocytes subclusters from Absinta et al, Nature 2021, showed higher *TSPO* expression in neurodegenerative glial phenotypes. Abbreviations: AST = astrocytes; ENDOTH = endothelial cells; IMM = immune cells; MS = multiple sclerosis; NEU = neurons; OLIGO = oligodendrocytes; OPC = oligodendrocytes precursor cells; *TSPO* = translocator protein 18 kDa gene; VAS = other vascular cells. [Color figure can be viewed at www.annalsofneurology.org]

inflamed in MS or AIMS, z-scores of 2.6 relative to all astrocytes; see Figure 5E).

Discussion

In this prospective longitudinal study combining [18F]-DPA-714-PET and MRI, we propose an optimized in vivo classification of WM MS lesions based on innate immune cell content and localization, which allowed us to identify whether each plaque was characterized or not by a smoldering neuroinflammatory component. Although all lesions we analyzed appeared inactive on conventional MRI (no contrast uptake), we found that most of them were characterized by a smoldering component, either homogeneous or restricted to lesion rims, particularly in

patients with progressive disease. Moreover, we found that the number of lesions with a smoldering component detectable with TSPO-PET significantly predicted neurodegeneration and clinical progression over 2 years. These results highlight the interest of the classification of individualized lesions according to their inflammatory component.

To ensure a reliable classification of lesions, we applied an optimized methodological approach. First, PVE was corrected and minimized by investigating only sub-lesional areas (ie, lesion rims and centers) greater than the resolution of our PET system. Second, the classification of sub-lesional areas we propose here was based on data-driven calculated thresholds. Finally, as CALs may predominate near the ventricles where lesions are often confluent,[15] we implemented a segmentation method to separate individual lesions within an area of confluence.[33] This approach revealed that, in our cohort of patients with MS with a relatively high disease duration (9 ± 6 years), most of gadolinium negative lesions maintained a persisting smoldering neuroinflammatory component, whether extended throughout the lesion (homogeneously active lesions) or confined to the lesional rim (rim-active lesions). This finding supports the notion that following acute inflammation and demyelination, the fate of each single lesion may dynamically evolve over several years in vivo.

In their post mortem study, Luchetti and colleagues[5] identified in autopsy cases up to 30% of mixed active/inactive lesions for patients with MS. Similar to our results, these chronic lesions were more common in male patients and in subjects with a progressive form of the disease but could also be detected in RRMS. Frischer et al,[7] who also detected a persisting macrophagic/microglial component in the majority of post mortem lesions, including late active lesions and chronic active lesions, highlighted a subtype of these lesions, named slowly expanding/smoldering lesions (reminding mixed active-inactive lesions), characterized by an inactive center surrounded by a thin rim of activated microglia, which were not detected in people with RRMS at the post mortem stage. This latter result suggested that patients who die without having converted to progressive MS might be those who have not accumulated slowly expanding lesions (SEL) and smoldering lesions during the course of their disease, supporting the notion that this lesion subtype may be a possible risk factor of a more severe clinical evolution. Of note, the lesion stage described in our study as homogeneously active has not yet been fully described in post mortem studies. One hypothesis is that they represent an intermediate stage between late active lesions and mixed active/inactive lesions. In the seminal description of

lesion subtypes by Frischer et al,[7] the combination of these 2 types of active lesions reached a proportion of nearly 60% for patients with 1 to 5 years disease duration, and 50% for patients with 5 to 10 years disease duration, which fit well with our results. With longer disease durations, the proportion of late active lesions was decreasing (to almost disappear after 30 years) whereas the proportion of mixed active/inactive was slightly increasing.[7] This evolution is consistent with the hypothesis of an intermediate lesional stage being captured as "homogeneously active lesions" with ^{18}F-DPA-714 PET.

Several imaging studies have recently attempted to visualize CALs and persisting neuroinflammation in MS.[17,37] Susceptibility weighted MRI sequences allow to capture a subset of lesions with a perilesional paramagnetic rim. This rim is thought to reflect the presence of chronically activated microglia, which has the particularity to be rich in iron (a paramagnetic component). First developed at 7 T,[42] this method has now been adapted for 3 T and 1.5 T MRI, and a threshold of 4 brain rim positive lesions has been shown to associate with a worse clinical evolution.[43] Studies combining pathology and MRI confirmed that paramagnetic perilesional rims are associated with iron-rich microglial accumulation in CAL.[9,16] Building on the concept that perilesional microglial activation might result in slow lesion expansion in a subset of lesions,[9] slowly expansion lesions or SELs, which are lesions defined by a slow, constant and concentric volume increase over time, have been identified in vivo with a Jacobian integration method.[15] The number of MRI-defined SELs was then shown to be associated with neurological disability and ongoing tissue damage within lesions on T1-weighted sequences.[44] Of note, using a recently described method for single-voxel classification based on TSPO binding,[25] PET with ^{11}C-PK11195 could also identify active lesions and rim-positive lesions, with the latter lesion subtype being significantly correlated with clinical scores in a cross-sectional analysis.[26]

We found here that homogeneously active lesions played a predominant role in atrophy progression and disability worsening over 2 years. Added to the results of previous MRI and PET studies on rim-active lesions, our findings support the notion that the persisting immune cell activation within lesions at the subacute/chronic stage, both if extended throughout the plaque or confined to its rim, critically shapes the process of neurodegeneration and clinical progression in MS. Interestingly, the proportion of homogeneously active lesions did not differ according to treatment or between patients with RRMS and PMS. Moreover, their predictive value was maintained even among subjects without any MRI activity or relapse during the follow-up, suggesting that they developed mostly

independently of the adaptive inflammatory process, and may represent a substrate of progression independent of relapses.[4] The biological reasons underlying persisting innate immune cell activation in MS lesions remains unknown. Microglial cells could play a beneficial role in the acute/subacute stage of lesions, by clearing potentially toxic debris and promoting repair.[6] However, as lesions and disease progress, cellular homeostasis is disrupted, and microglia mostly adopt a pro-inflammatory, degeneration-associated fate.[10,11,36] At the cellular level, the persistence of pro-inflammatory microglia may involve a dysfunction of the biosynthetic pathway of pro-resolving lipid mediators.[45] At a larger scale, we also demonstrated that chronic neuroinflammation follows a gradient depending on the proximity to the ventricles, as active lesions accumulate in the periventricular WM in this study, reinforcing the previous demonstration of a periventricular gradient of neuroinflammation at the voxel level.[37] This regionalization suggests a possible dysfunction at the brain-to-CSF barrier (BCSFB) level. Fitting with this hypothesis, we found a close association between the volume of choroid plexuses and the percentage of homogeneously active lesions within the brain, the correlation being stronger in the first periventricular white matter rim. Choroid plexuses are unique interfaces contributing to immunosurveillance regulation.[12] They have been shown to be enlarged and inflamed in patients with MS, particularly in those with RRMS and inflammatory profiles,[13] and this enlargement was already detected at the pre-symptomatic stage of MS.[46] Their dysfunction could therefore participate locally to the persistence of pro-inflammatory microglial activation, by promoting local antigen presentation by innate immune cells expressing CD163,[46] and/or inhibiting the selective recruitment of inflammation-resolving leukocytes to the inflamed brain.[12] Interestingly, a similar selective periventricular failure of remyelination within WM lesions has been recently demonstrated, and this failure associated with CP enlargement,[47] suggesting that persisting microglial inflammation and failure of myelin repair are interconnected processes that synergistically contribute to neurodegeneration. Similarly, CAL are characterized by axonal injury/loss and poor repair capacities on both post mortem samples[48] and in vivo longitudinal studies.[49] This repair failure does not depend on intrinsic oligodendroglia factors but rather results from immune cell-derived extrinsic factors.[50,51] Taken together, all these results support the hypothesis that a dysfunction of the BCSFB may contribute to the persistence of neuroinflammation in subacute and chronic MS lesions, particularly in periventricular regions, resulting in a failure of myelin repair and tract-mediated neuronal damage that contribute to irreversible neurological disability.

Translating to the clinical settings an imaging approach capable of capturing the whole spectrum of lesions characterized by a smoldering component (including not only rim-active but also homogeneously active plaques), should enable to refine individual prognosis and to adapt personalized treatments. The 2 CAL subtypes we identified with PET may indeed reflect different stages of the neurodegenerative process. Rim-active lesions predominate in progressive MS when analyzed as an absolute number, whereas the difference did not remain significant when analyzed as a proportion of total T2 lesions. This discrepancy may be partly explained by the large variation of T2 lesion number found across subjects. Rim-active lesions tend to accumulate with older age, and are cross-sectionally associated with a reduced cortical volume at baseline. These results suggest that this particular subset of lesions could reflect a more advanced degenerative process and a shift toward a progressive form of MS at the clinical level. Homogeneously active lesions may instead reflect a dynamic process taking place at an earlier stage of the disease in a large proportion of lesions and triggering the degenerative cascade, as this type of plaque is best associated with the development of atrophy and clinical worsening over time. Whether quantitative MRI sequences may succeed in identifying these lesion subtypes remains an open question. In a recent classification of individual lesions based on quantitative susceptibility mapping (QSM) signal, 52% were characterized by diffuse hyperintensity, whereas 13% showed a perilesional rim.[52] When combined with histology, hyperintense QSM lesions were mostly inactive demyelinated lesions, but 28% still had an active neuroinflammatory component.[40] Combining TSPO-PET and multimodal MRI, it would therefore be intriguing to explore whether a subset of these hyperintense QSM lesions indeed corresponds to PET-defined CAL. This combination could also improve the biological characterization of lesions described as presenting a core sign on susceptibility-weighted imaging,[53] and would further decipher multimodal MRI signature of PET-defined CAL at baseline and in longitudinal studies (especially to explore the overlap between SEL and PET-defined CAL).

Our work has some limitations. First, the limited number of patients we included may reduce the power to detect the predictive value of some PET-derived metrics with minor effect, such as neuroinflammation in normal-appearing tissues. Second, the TSPO radiopharmaceutical binding, although reflecting mainly innate immune cell density, does not allow to fully discriminate between innate immune cell activation states and could also target

astrocytes within lesions.[19] However in post mortem studies, it was shown that astrocytes account for less than 5% of TSPO expression in active MS lesions.[54] Our investigation of single-nucleus RNAseq databases[34–36] further highlighted that in the MS brain the main *TSPO* expression was driven by activated microglia phenotypes, namely MIMS-iron followed by MIMS-foamy, and also indicated that the astrocyte component was characterized by a neurodegenerative inflamed astrocytes phenotype (AIMS). These results corroborate that the higher ^{18}F-DPA-7A4 binding characterizing both the rim active lesions and the core of homogeneously active lesions results from an increased density of pro-inflammatory cells, that may consist mainly of microglia but potentially also include a minor proportion of inflamed astrocytes, both cellular types contributing to the smoldering component of lesions.

In conclusion, [^{18}F]-DPA-714-PET allowed to classify WM MS lesions according to activated innate immune cells density and localization, and to unravel a persisting smoldering component within most of non-gadolinium enhanced lesions. Over a follow-up of 2 years, the proportion of homogeneously active lesions had the greatest predictive value on subsequent neurodegeneration and disability. Our results encourage reconsidering the prognostic value of MS lesion phenotypes on disease trajectories, in light of their heterogeneity regarding persisting neuroinflammation and repair. Identifying the multimodal MRI signatures of chronic active lesions subtypes would open the perspective of improving patient monitoring and personalized care.

Acknowledgments

Author Contributions

M.H., J.G., M.B., B.B., and B.S. contributed to the conception and design of the study. M.H., J.G., G.B., A.L., M.A., V.A.G.R., T.S., M.T., A.B., C.L., P.G., M.B., B.B., and B.S. contributed to the acquisition and analysis of data. M.H., J.G., G.B., M.T., B.B., and B.S. contributed to drafting the text or preparing the figures.

Potential Conflicts of Interest

The authors have no conflicts of interest to disclose related to the submitted work. Outside of the present work, M.H., J.G., G.B., A.L., T.S., M.T., P.G., A.B., and M.B., have nothing to disclose. M.A. received consultancy honoraria from Abata Therapeutics, Biogen, Sanofi-Genzyme, and GSK. V.A.G.R. reports fees for traveling from Biogen, Novartis, and Roche, speaker's honoraria from Novartis and personal fees from Biogen, Merck M3 Global Research, and Atheneum Partners. C.L. has received consulting or travel fees from Biogen, Novartis, Roche, Sanofi, Teva, and Merck Serono, and research grant from Biogen. B.B. reports fees for traveling and speaker's honoraria from Novartis, Genzyme, Roche, and Merck Serono. B.S. reports research support from Roche, Sanofi, and Merck and personal fees for lectures or advisory boards from Novartis, Sanofi, Biogen, Janssen, and Merck.

Data Availability

The data that support the findings of this study are available from the corresponding author upon reasonable request.

References

1. De Stefano N et al. Evidence of axonal damage in the early stages of multiple sclerosis and its relevance to disability. Arch Neurol 2001; 58:65–70.

2. Trapp BD, Peterson J, Ransohoff RM, et al. Axonal transection in the lesions of multiple sclerosis. N Engl J Med 1998;338:278–285.

3. Lassmann H. What drives disease in multiple sclerosis: inflammation or neurodegeneration? Clin Exp Neuroimmunol 2010;1:2–11.

4. Kappos L, Wolinsky JS, Giovannoni G, et al. Contribution of relapse-independent progression vs relapse-associated worsening to overall confirmed disability accumulation in typical relapsing multiple sclerosis in a pooled analysis of 2 randomized clinical trials. JAMA Neurol 2020;77:1132–1140.

5. Luchetti S, Fransen NL, van Eden CG, et al. Progressive multiple sclerosis patients show substantial lesion activity that correlates with clinical disease severity and sex: a retrospective autopsy cohort analysis. Acta Neuropathol (Berl.) 2018;135:511–528.

6. Lloyd AF, Miron VE. The pro-remyelination properties of microglia in the central nervous system. Nat Rev Neurol 2019;15:447–458.

7. Frischer JM, Weigand SD, Guo Y, et al. Clinical and pathological insights into the dynamic nature of the white matter multiple sclerosis plaque. Ann Neurol 2015;78:710–721.

8. Kuhlmann T, Ludwin S, Prat A, et al. An updated histological classification system for multiple sclerosis lesions. Acta Neuropathol (Berl) 2017;133:13–24.

9. Dal-Bianco A, Grabner G, Kronnerwetter C, et al. Slow expansion of multiple sclerosis iron rim lesions: pathology and 7 T magnetic resonance imaging. Acta Neuropathol (Berl.) 2017;133:25–42.

10. Zrzavy T, Hametner S, Wimmer I, et al. Loss of 'homeostatic' microglia and patterns of their activation in active multiple sclerosis. Brain 2017;140:1900–1913.

11. Yong VW. Microglia in multiple sclerosis: protectors turn destroyers. Neuron 2022;110:3534–3548. https://doi.org/10.1016/j.neuron.2022.06.023.

12. Schwartz M, Baruch K. The resolution of neuroinflammation in neurodegeneration: leukocyte recruitment via the choroid plexus. EMBO J 2014;33:7–22.

13. Ricigliano VAG. Choroid Plexus Enlargement in Inflammatory Multiple Sclerosis: 3.0-T MRI and Translocator Protein PET Evaluation | Radiology, https://pubs.rsna.org/doi/10.1148/radiol.2021204426.

14. Fleischer V, Gonzalez-Escamilla G, Ciolac D, et al. Translational value of choroid plexus imaging for tracking neuroinflammation in mice and humans. Proc Natl Acad Sci U S A 2021;118:e2025000118.

15. Elliott C, Wolinsky JS, Hauser SL, et al. Slowly expanding/evolving lesions as a magnetic resonance imaging marker of chronic active multiple sclerosis lesions. Mult Scler J 2019;25:1915–1925.

16. Kaunzner UW, Kang Y, Zhang S, et al. Quantitative susceptibility mapping identifies inflammation in a subset of chronic multiple sclerosis lesions. Brain J Neurol 2019;142:133–145.

17. Calvi A, Haider L, Prados F, et al. In vivo imaging of chronic active lesions in multiple sclerosis. Mult Scler J 2022;28:683–690.

18. Bodini B, Tonietto M, Airas L, Stankoff B. Positron emission tomography in multiple sclerosis — straight to the target. Nat Rev Neurol 2021;17:663–675.

19. Nutma E, Stephenson JA, Gorter RP, et al. A quantitative neuropathological assessment of translocator protein expression in multiple sclerosis. Brain J Neurol 2019;142:3440–3455.

20. Herranz E, Giannì C, Louapre C, et al. Neuroinflammatory component of gray matter pathology in multiple sclerosis. Ann Neurol 2016;80:776–790.

21. Colasanti A, Guo Q, Muhlert N, et al. In vivo assessment of brain white matter inflammation in multiple sclerosis with 18F-PBR111 PET. J Nucl Med 2014;55:1112–1118.

22. Datta G, Colasanti A, Kalk N, et al. 11C-PBR28 and 18F-PBR111 detect white matter inflammatory heterogeneity in multiple sclerosis. J Nucl Med 2017;58:1477–1482.

23. Sucksdorff M, Matilainen M, Tuisku J, et al. Brain TSPO-PET predicts later disease progression independent of relapses in multiple sclerosis. Brain 2020;143:3318–3330.

24. Rissanen E, Tuisku J, Vahlberg T, et al. Microglial activation, white matter tract damage, and disability in MS. Neurol Neuroimmunol Neuroinflamm 2018;5:e443.

25. Bodini B, Poirion E, Tonietto M, et al. Individual mapping of innate immune cell activation is a candidate marker of patient-specific trajectories of worsening disability in multiple sclerosis. J Nucl Med 2020;61:1043–1049.

26. Nylund M, Sucksdorff M, Matilainen M, et al. Phenotyping of multiple sclerosis lesions according to innate immune cell activation using 18 kDa translocator protein-PET. Brain Commun 2022;4:fcab301.

27. García-Lorenzo D, Lavisse S, Leroy C, et al. Validation of an automatic reference region extraction for the quantification of [18F]DPA-714 in dynamic brain PET studies. J Cereb Blood Flow Metab 2018;38:333–346.

28. Polman CH, Reingold SC, Edan G, et al. Diagnostic criteria for multiple sclerosis: 2005 revisions to the "McDonald criteria". Ann Neurol 2005;58:840–846.

29. Owen DR, Yeo AJ, Gunn RN, et al. An 18-kDa translocator protein (TSPO) polymorphism explains differences in binding affinity of the PET Radioligand PBR28. J Cereb Blood Flow Metab 2012;32:1–5.

30. Benedict RH, DeLuca J, Phillips G, et al. Validity of the symbol digit modalities test as a cognition performance outcome measure for multiple sclerosis. Mult Scler 2017;23:721–733.

31. Cadavid D, Cohen JA, Freedman MS, et al. The EDSS-plus, an improved endpoint for disability progression in secondary progressive multiple sclerosis. Mult Scler J 2017;23:94–105.

32. Dworkin JD, Linn KA, Oguz I, et al. An automated statistical technique for counting distinct multiple sclerosis lesions. AJNR Am J Neuroradiol 2018;39:626–633.

33. Nakamura K, Guizard N, Fonov VS, et al. Jacobian integration method increases the statistical power to measure gray matter atrophy in multiple sclerosis. NeuroImage Clin 2014;4:10–17.

34. Jäkel S, Agirre E, Mendanha Falcão A, et al. Altered human oligodendrocyte heterogeneity in multiple sclerosis. Nature 2019;566:543–547.

35. Schirmer L, Velmeshev D, Holmqvist S, et al. Neuronal vulnerability and multilineage diversity in multiple sclerosis. Nature 2019;573:75–82.

36. Absinta M, Maric D, Gharagozloo M, et al. A lymphocyte–microglia–astrocyte axis in chronic active multiple sclerosis. Nature 2021;597:709–714.

37. Poirion E, Tonietto M, Lejeune FX, et al. Structural and clinical correlates of a periventricular gradient of Neuroinflammation in multiple sclerosis. Neurology 2021;96:e1865–e1875.

38. Sumowski JF, Benedict R, Enzinger C, et al. Cognition in multiple sclerosis: state of the field and priorities for the future. Neurology 2018;90:278–288.

39. Magnin E, Sagawa Y, Moulin T, Decavel P. What are the minimal detectable changes in SDMT and verbal fluency tests for assessing changes in cognitive performance in persons with multiple sclerosis and non-multiple sclerosis controls? Eur Neurol 2020;83:263–270.

40. Eijlers AJC, Dekker I, Steenwijk MD, et al. Cortical atrophy accelerates as cognitive decline worsens in multiple sclerosis. Neurology 2019;93:e1348–e1359.

41. Stefano ND et al. Establishing pathological cut-offs of brain atrophy rates in multiple sclerosis. J Neurol Neurosurg Psychiatry 2016;87:93–99.

42. Hammond KE, Metcalf M, Carvajal L, et al. Quantitative in vivo magnetic resonance imaging of multiple sclerosis at 7 tesla with sensitivity to iron. Ann Neurol 2008;64:707–713.

43. Absinta M, Sati P, Masuzzo F, et al. Association of Chronic Active Multiple Sclerosis Lesions with Disability In Vivo. JAMA Neurol 2019;76:1474–1483.

44. Elliott C, Belachew S, Wolinsky JS, et al. Chronic white matter lesion activity predicts clinical progression in primary progressive multiple sclerosis. Brain J Neurol 2019;142:2787–2799.

45. Zahoor I, Giri S. Specialized pro-resolving lipid mediators: emerging therapeutic candidates for multiple sclerosis. Clin Rev Allergy Immunol 2021;60:147–163.

46. Ricigliano VAG. Imaging characteristics of choroid plexuses in presymptomatic multiple sclerosis: a retrospective study. Neurol Neuroimmunol Neuroinflamm 2022;9(6):e200026.

47. Tonietto M. Periventricular failure of remyelination in multiple sclerosis: a subtrate for neurodegeneration. Brain 2022;146:182–194.

48. Heß K, Starost L, Kieran NW, et al. Lesion stage-dependent causes for impaired remyelination in MS. Acta Neuropathol (Berl.) 2020;140:359–375.

49. Absinta M, Sati P, Schindler M, et al. Persistent 7-tesla phase rim predicts poor outcome in new multiple sclerosis patient lesions. J Clin Invest 2016;126:2597–2609.

50. Starost L, Lindner M, Herold M, et al. Extrinsic immune cell-derived, but not intrinsic oligodendroglial factors contribute to oligodendroglial differentiation block in multiple sclerosis. Acta Neuropathol (Berl.) 2020;140:715–736.

51. El Behi M et al. Adaptive human immunity drives remyelination in a mouse model of demyelination. Brain J Neurol 2017;140:967–980.

52. Rahmanzadeh R, Galbusera R, Lu PJ, et al. A new advanced MRI biomarker for Remyelinated lesions in multiple sclerosis. Ann Neurol 2022;92:486–502.

53. Blindenbacher N et al. Evaluation of the 'ring sign' and the 'core sign' as a magnetic resonance imaging marker of disease activity and progression in clinically isolated syndrome and early multiple sclerosis. Mult Scler J Exp Transl Clin 2020;6:2055217320915480.

54. Nutma E, Gebro E, Marzin MC, et al. Activated microglia do not increase 18 kDa translocator protein (TSPO) expression in the multiple sclerosis brain. Glia 2021;69:2447–2458.